AJNR

This information is current as of August 20, 2025.

Multiparametric Characterization and Spatial Distribution of Different MS Lesion Phenotypes

Francesco Tazza, Giacomo Boffa, Simona Schiavi, Caterina Lapucci, Gian Franco Piredda, Emilio Cipriano, Domenico Zacà, Luca Roccatagliata, Tom Hilbert, Tobias Kober, Matilde Inglese and Mauro Costagli

Multiparametric Characterization and Spatial Distribution of Different MS Lesion Phenotypes

Francesco Tazza, Giacomo Boffa, Simona Schiavi, Caterina Lapucci, Gian Franco Piredda, Emilio Cipriano, Domenico Zacà, Luca Roccatagliata, Tom Hilbert, Tobias Kober, Matilde Inglese, and Mauro Costagli

ABSTRACT

BACKGROUND AND PURPOSE: MS lesions exhibit varying degrees of axonal and myelin damage. A comprehensive description of lesion phenotypes could contribute to an improved radiologic evaluation of smoldering inflammation and remyelination processes. This study aimed to identify in vivo distinct MS lesion types using quantitative susceptibility mapping and susceptibility mapping–weighted imaging and to characterize them through T1-relaxometry, myelin mapping, and diffusion MR imaging. The spatial distribution of lesion phenotypes in relation to ventricular CSF was investigated.

MATERIALS AND METHODS: MS lesions of 53 individuals were categorized into iso- or hypointense lesions, hyperintense lesions, and paramagnetic rim lesions, on the basis of their appearance on quantitative susceptibility mapping alone, according to published criteria, and with the additional support of susceptibility mapping–weighted imaging. Susceptibility values, T1-relaxation times, myelin and free water fractions, intracellular volume fraction, and the orientation dispersion index were compared among lesion phenotypes. The distance of the geometric center of each lesion from the ventricular CSF was calculated.

RESULTS: Eight hundred ninety-six MS lesions underwent the categorization process using quantitative susceptibility mapping and susceptibility mapping–weighted imaging. The novel use of susceptibility mapping–weighted images, which revealed additional microvasculature details, led us to re-allocate several lesions to different categories, resulting in a 35.6% decrease in the number of paramagnetic rim lesions, a 22.5% decrease in hyperintense lesions, and a 17.2% increase in iso- or hypointense lesions, with respect to the categorization based on quantitative susceptibility mapping only. The outcome of the categorization based on the joint use of quantitative susceptibility mapping and susceptibility mapping–weighted imaging was that 44.4% of lesions were iso- or hypointense lesions, 47.9% were hyperintense lesions, and 7.7% were paramagnetic rim lesions. A worsening gradient was observed from iso- or hypointense lesions to hyperintense lesions to paramagnetic rim lesions in T1-relaxation times, myelin water fraction, free water fraction, and intracellular volume fraction. Paramagnetic rim lesions were located closer to ventricular CSF than iso- or hypointense lesions. The volume of hyperintense lesions was associated with a more severe disease course.

CONCLUSIONS: Quantitative susceptibility mapping and susceptibility mapping–weighted imaging allow in vivo classification of MS lesions into different phenotypes, characterized by different levels of axonal and myelin loss and spatial distribution. Hyperintense lesions and paramagnetic rim lesions, which have the most severe microstructural damage, were more often observed in the periventricular WM and were associated with a more severe disease course.

ABBREVIATIONS: ARMSS = Age-Related MS Severity Score; EDSS = Expanded Disability Status Scale; FWF = free water fraction; HC = healthy control; HYPER = hyperintense lesions; ISO-HYPO = iso- or hypointense lesions; ICVF = intracellular volume fraction; MWF = myelin water fraction; ODI = orientation dispersion index; PRL = paramagnetic rim lesion; QSM = quantitative susceptibility mapping; SMWI = susceptibility mapping–weighted imaging

Multiple sclerosis is a chronic inflammatory demyelinating neurodegenerative disease of the CNS characterized by the occurrence of multifocal and widespread brain and spinal cord lesions. After the acute inflammatory demyelinating phase, MS

SUMMARY

PREVIOUS LITERATURE: Quantitative susceptibility mapping has been proposed for lesion characterization in multiple sclerosis. Iso- and hypointense lesions in QSM have been linked to remyelinated lesions, while paramagnetic rim lesions may serve as biomarkers for chronic active lesions. To date, the characterization of hyperintense lesions without a rim pattern is incomplete. As veins can prevent accurate characterization of lesions in QSM, susceptibility mapping–weighted imaging may be used for optimal visualization of vessels within or adjacent to MS lesions. Last, a detrimental effect of CSF has been proposed as a pathogenetic mechanism in MS.

KEY FINDINGS: SMWI significantly improved vein visualization, leading to several lesion reclassifications with respect to the use of QSM only. ISO-HYPO lesions had the least severe structural damage, while PRLs and HYPER lesions showed the worst degree of damage, correlated with greater disability, and were located more closely to the ventricles.

KNOWLEDGE ADVANCEMENT: MS lesion assessment based on the combined use of QSM and SMWI may improve lesion phenotyping. HYPER lesions exhibit characteristics of severe structural damage and may contribute to patient disability, which warrants further investigation.

lesions can follow diverse trajectories across time, including resolution of inflammation, persistence of microglia-induced neuroinflammation, irreversible demyelination, or efficient myelin repair. Kuhlmann et al[1] have proposed a classification of MS lesions as active, chronically active, and inactive lesions, with or without ongoing demyelination. Yet, determinants driving the evolution of MS lesions remain unknown. According to the "surface-in" pathologic hypothesis,[2] the ventricular and peripheral CSF entails microstructural damage involving, respectively, the periventricular lesional and extra-lesional WM[3,4] and the outer layer of cortical GM.[5] Particularly, a periventricular gradient of neuroinflammation likely mediated by the innate immune system has been demonstrated.[6]

Quantitative MR imaging has the potential to disentangle the heterogeneity of MS lesions in vivo, which is important for treatment and monitoring. Quantitative susceptibility mapping (QSM)[7] has recently emerged as a valuable technique to categorize MS lesions because it may reflect the level of demyelination and inflammation. In a combined MR imaging–histopathologic study, iso- and hypointense QSM lesions exhibited 100% specificity for remyelinated lesions,[8] while 95% of lesions with a QSM hyperintense rim (called paramagnetic rim lesions [PRLs]) corresponded to chronically active lesions. Conversely, QSM hyperintense lesions without a rim pattern demonstrated more heterogeneity and lack of a proper characterization. Therefore, providing a multiparametric description of QSM phenotypes (hypo-, iso-, and hyperintense lesions with and without a rim) within the same cohort of patients could contribute to a more in-depth characterization of the patient's specific disease stage beyond the clinical status and an improved radiologic monitoring, particularly of smoldering inflammation and remyelination.

PRLs constitute from 2.3% to 41.0% of the MS lesions according to a recent meta-analysis.[9] Different factors may contribute to the variation observed, such as the MS phenotype, disease duration, or clinical severity of the cohorts included. Nevertheless, some of this variability may be a result of methodologic disparities in the definition of PRLs,[10] as well as of lesion misclassification using solely QSM which, for example, may not consistently discern the hyperintense signal due to the presence of vessels in

proximity to the lesions. This issue is particularly relevant in vein-rich brain areas, like the periventricular regions, where most of the MS lesions are located. This aspect has been addressed in the most recent consensus statement on the definition of PRLs, cautioning about the potential resemblance of veins running alongside rims to rims themselves.[10] Susceptibility mapping-weighted imaging (SMWI) is an MR imaging technique with superb vascular contrast and with significantly reduced artifacts ascribable to the nonlocal properties of phase images compared with conventional SWI.[11] Consequently, SMWI could be a valuable tool for optimal visualization of vessels within or bordering MS lesions, improving the assessment of PRLs and hyperintense lesions on QSM.

The objective of this study was twofold. First, we aimed to characterize WM MS lesions on the basis of QSM and SMWI intensity patterns and assess their tissue microstructure using a quantitative T1-relaxation time,[12,13] myelin,[8] and diffusion imaging maps.[14] Alterations in tissue T1-relaxation are attributable to varying concentrations of water, proteins, and paramagnetic substances, in particular iron. In the context of MS lesions, it has been proposed that longer T1 values correlate with demyelination and axonal loss, while shorter values are suggestive of partial or complete remyelination.[13] Of note, a direct correlation between T1-relaxation times and the QSM signal pattern has not yet been demonstrated. Higher myelin water fraction (MWF) values are associated with higher tissue myelin content, while higher free water fraction (FWF) values are commonly related to increased tissue water content, such as in edema and inflammation.[15] By means of diffusion imaging, lower intracellular volume fraction (ICVF) and higher orientation dispersion index (ODI) values have been related to loss of coherence of axonal fibers, demyelination, and microstructural neuronal damage. The second aim of this study was to investigate the spatial distribution of distinct WM MS lesion types in relationship to the proximity to ventricular CSF and to assess their association with disability and disease severity.

MATERIALS AND METHODS
Study Population and Design
We prospectively collected cross-sectional data from 53 patients with MS and 24 healthy controls (HCs) at our MS center. All
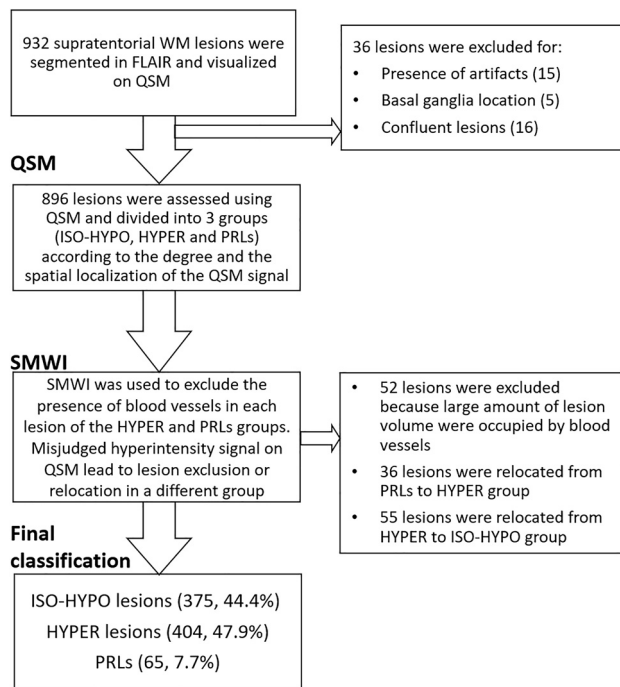
FIG 1. Flow chart of the MS lesions evaluation based on QSM and SMWI visualization.

participants were 18 years of age or older. Inclusion criteria for patients with MS were the following: 1) 18 years of age or older; 2) diagnosis of relapsing-remitting MS or secondary-progressive MS according to the 2017 McDonald criteria; 3) absence of clinical relapse, MR imaging activity, and steroid treatment in the last 6 months. Exclusion criteria were the following: 1) the presence of other neurologic comorbidities, and 2) contraindications to MR imaging. For all included patients, disease- and treatment-related data were collected. All subjects were scanned with a 3T MR imaging scanner (Magnetom Prisma; Siemens) using a 64-channel head/neck coil. The MR imaging protocol included the following:

- 3D FLAIR (TR/TE/TI = 5000/393/1800 ms, field of view = 256 mm, matrix size = 320, interpolated resolution = 0.4 × 0.4 × 1 mm^3), used for lesion segmentation
- MP2RAGE[16] research application (TR/TE/TI1/TI2 = 5000/2.9/700/2500 ms, resolution = 1 mm isotropic, 4.6× accelerated with compressed sensing) used for T1-weighted structural imaging, brain tissue segmentation, and quantitative T1 mapping
- Multiecho gradient-spin-echo[17] (GRASE) research application (TR = 1000 ms, 32 TE between 10.36 and 331.52 ms, transversal acquisition with resolution = 1.8 × 1.8 × 1.8 mm^3, controlled aliasing in parallel imaging results in higher acceleration (CAIPIRINHA) 3 × 2$^{(1)}$, used for myelin mapping and computation of intra-/extra-axonal T2 values
- Segmented 3D EPI[18] (TR/TE = 64/35 ms, resolution = 0.65 mm isotropic), used for QSM and SMWI
- Multishell diffusion MRI[19,20] with b-values = 300 s/mm^2 (3 directions), 700 s/mm^2 (7 directions), 1000 s/mm^2 (16 directions), 2000 s/mm^2 (29 directions), and 3000 s/mm^2 (46 directions), and 7 measurements of b-value = 0 s/mm^2 interspersed throughout the acquisition, followed by 7 measurements of

b-value = 0 s/mm^2 with reversed phase-encoding (TR/TE = 4600/75 ms, resolution = 1.8 mm isotropic), used for tissue microstructure characterization.

This study was approved by the local ethics committee, and written consent was obtained from all subjects.

### MR Imaging Data Processing and Analyses
The processing and analysis flow chart of this study is graphically represented in Fig 1 and follows the Strengthening the Reporting of Observational Studies in Epidemiology (STROBE) guidelines.[21]

MS Lesion Classification Using Susceptibility Imaging
T2-hyperintense and T1-hypointense lesions were segmented on FLAIR and T1-weighted images, respectively, using a semiauto-mated segmentation technique based on user-supervised local thresholding (SinLab; Siena Imaging; https://sinlab-rhb.sienaimaging. com/). Lesions <0.03 mL were excluded from further analyses. QSM images were computed from 3D EPI using a custom set of codes in Matlab (MathWorks) using STI Suite routines (https://people.eecs. berkeley.edu/~chunlei.liu/software.html) for image phase-unwrapping,[22] background phase removal,[23] and dipole deconvolution.[24] Quantitative susceptibility values obtained via this pipeline are implicitly referenced to the whole-brain mask.[25] SMWI was obtained by merging the EPI signal-intensity images and quantitative susceptibility maps according to a previously documented pipeline[24] with parameters χ_{th} = 1 part per million and m = 4. FLAIR images were registered to the corresponding EPI magnitude images using the FMRIB Linear Image Registration Tool (FLIRT; http://www.fmrib. ox.ac.uk/),[26] and the derived transformations were combined to register MS WM lesion masks to the QSM/SMWI space. On the basis of QSM images, we excluded lesions with the following features: 1) lesions in regions with obvious susceptibility artifacts (ie, the orbitofrontal region or close to the temporal poles) and infratentorial lesions, whose visualization is unclear in QSM;[10] 2) lesions involving the basal ganglia, which are intrinsically hyperintense on QSM; and 3) confluent lesions showing multiple inhomogeneous patterns of QSM signal, impeding a clear-cut classification. Using both QSM and SMWI, 2 independently trained professionals with >5 years of experience in MS neuroimaging (F.T. and G.B.) visually classified the MS lesions. In case of disagreement between the 2 raters, a consensus was reached in a second evaluation.

The QSM signal was used to classify WM lesions as hyperin-tense versus nonhyperintense. The latter includes both isointense lesions and hypointense lesions on QSM (ISO-HYPO), which showed a susceptibility not greater than that of surrounding normal-appearing WM. Hyperintense lesions, which showed higher susceptibility than the surrounding normal-appearing WM, were subsequently divided into 2 subgroups, according to their hyperintensity pattern: 1) PRLs, characterized by the presence of a hyperintense rim with respect to the center; and 2) hyperintense lesions (HYPER), characterized by a diffuse (either homogeneous or inhomogeneous) distribution of hyperintensity within the whole lesion. To better visualize veins, which are a potential confound for lesion classification due to their hyperintense appearance in QSM, we visually inspected SMWI to exclude the presence of blood vessels in QSM-hyperintense lesions. Lesions in which the confounding effect of blood vessels was not ruled out by SMWI inspection were
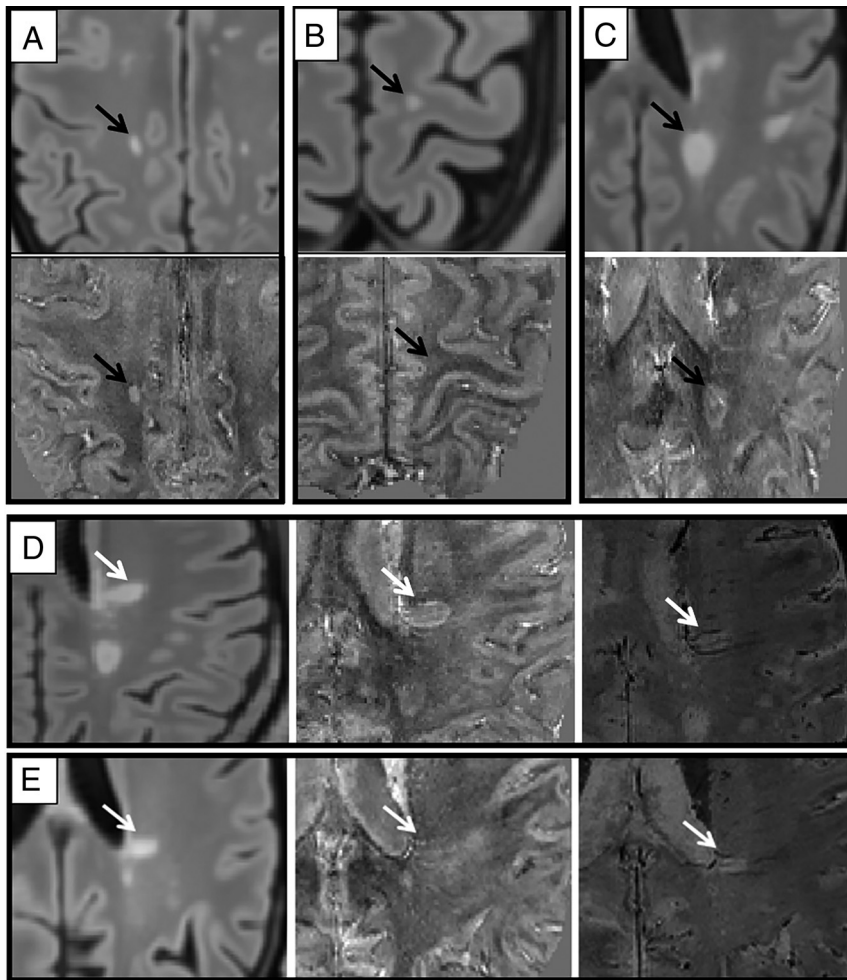
FIG 2. Examples of different MS lesion phenotypes. *A*, *B*, and *C*, MS lesions (*black arrow*) on FLAIR (*upper image*) and on QSM (*lower image*) classified, respectively, in HYPER, ISO-HYPO, and PRLs groups. *D* and *E*, MS lesions (*white arrows*) on FLAIR (*left*), QSM (*center*), and SMWI (*right*), which were relocated, respectively, from PRLs to HYPER and from HYPER to ISO-HYPO groups; particularly in *D*, the hyperintense rim on QSM was determined to be composed of 2 veins (visible as hypointense signal in SMWI). *E*, The hyperintensity on QSM located at the center of the lesion was a central vein, as shown on SMWI.

excluded from further analyses. Figures 1 and 2 summarize our MS lesion classification approach.

Quantitative MR Imaging

Susceptibility Imaging. Magnetic susceptibility can assume a relatively broad range of physiologic values across the brain,[27] because the measured magnetic susceptibility values depend on the different physiologic local concentrations of magnetic compounds in tissues (above all, diamagnetic myelin and paramagnetic iron) and on the orientation of the principal fiber tracts.[28] Therefore, rather than studying the raw QSM values in lesions, we evaluated the difference between the QSM values in each lesion and the corresponding values observed in the same region of a reference template based on the QSM data of the 24 HCs (16 women; mean age, 38 [SD, 13] years), acquired with the same parameters as those used for the patients with MS. Each HC's EPI T2*-weighted signal-intensity image was rigidly coregistered to the respective T1-weighted scan using FSL FLIRT, which was

then coregistered to the standard Montreal Neurological Institute 152 (MNI152) space using a combination of affine (FSL FLIRT) and nonlinear (FSL FNIRT; https://fsl.fmrib.ox.ac.uk/fsl/fslwiki/FNIRT) transformations.[26] The transformations were then applied to bring the subject's QSM to MNI152 space using nearest-neighbor interpolation.[26] The QSM reference template was finally obtained by voxelwise averaging of the coregistered HC's QSM data. The susceptibility values in patients' lesions were compared ROI-wise with the corresponding susceptibility values in the HC template coregistered to the individual MS patient, as follows:

$$QSM_{lesion} = mean_{i \in lesion}[QSM_{patient}(voxel_i) - QSM_{HCs}(voxel_i)],$$

where $voxel_i$ indicates the voxels of the lesion, $QSM_{patient}$ and QSM_{HCs} are the QSM maps of the patient in his or her original space and the QSM reference template coregistered to the patient's space, respectively. To validate lesion classification on the basis of visual assessment, we extracted and compared the QSM signal from each MS lesion subcategory.

Myelin Imaging. Multiecho GRASE images were processed using the multi-component-T2-toolbox (https://github.com/ejcanalesr/multicomponent-T2-toolbox). First, the images were corrected for Gibbs ringing and B_1-induced field inhomogeneities as previously described.[13] Then MWF and FWF maps were generated.[29]

Diffusion Imaging. Diffusion MR images were first denoised using the Marchenko-Pastur principal component analysis algorithm available in MRtrix3 (https://www.mrtrix.org/).[30] Then, they were corrected for movement artifacts and susceptibility-induced distortions using FSL commands topup (https://fsl.fmrib.ox.ac.uk/fsl/fslwiki/topup/TopupUsersGuide) and eddy (https://fsl.fmrib.ox.ac.uk/fsl/fslwiki/eddy/UsersGuide).[31] B_1 field inhomogeneity correction was applied to all the diffusion MRI volumes via the ANTs N4 algorithm (http://stnava.github.io/ANTs/).[32] To fit the neurite orientation dispersion and density imaging (NODDI) model,[33] we used the Accelerated Microstructural Imaging via Convex Optimization (AMICO) software (https://pypi.org/project/dmri-amico/),[34] and both ICVF and the ODI were obtained.

Table 1: Demographic and clinical features

	Patients with MS (n = 53)	Healthy Controls (n = 24)	P Value
Female (No.) (%)	34 (64.2%)	16 (66.7%)	.830
Mean age (yr)	43.64 (SD, 12.58)	38.12 (SD, 13.2)	.642
RRMS (No.) (%)	40 (75.5%)	NA	NA
Mean disease duration (yr)	9.91 (SD, 10.56)	NA	NA
EDSS (median) (range)	2.0 (0–7.0)	NA	NA
ARMSS (mean) (SD)	3.99 (SD, 2.32)	NA	NA
Treatment			
No therapy (No.) (%)	9 (17%)	NA	NA
Low-efficacy DMT (No.) (%)	10 (19%)	NA	NA
High-efficacy DMT (No.) (%)	34 (64%)	NA	NA

Note:—RRMS indicates relapsing-remitting MS; NA, not applicable; DMT, disease-modifying therapy.

T1-Relaxometry. Quantitative T1-relaxation maps were produced directly on the scanner from the MP2RAGE scan.[35]

MS Lesion Localization

The 3D Euclidean distance of each lesion center from the ventricular CSF was calculated, and distance maps were obtained using the FSL "distancemap" command as previously described, to investigate the proximity of different MS lesion phenotypes to the ventricles.[3]

Statistical Analysis

Lesion-wise statistical analyses were performed using SPSS (Version 28; IBM). Two-sided P values < .05 were considered significant. Descriptive results were reported as mean (SD) or median with interquartile range. The Shapiro-Wilk test and visual inspection of the histograms were performed to evaluate variable distributions. To compare the differences in quantitative measures and the distance from the ventricles among the different types of MS lesions, we conducted an ANOVA with Bonferroni post hoc comparisons, controlling for age, sex, and lesion volume as confounding factors. To account for the lack of statistical independence among results for MS lesions in the same patient, we incorporated an anonymized subject identification as a control variable. ANOVA was used to assess differences in MS lesion phenotype volume among MS phenotypes and between men and women, including the total lesion volume as a confounding factor. Pearson correlation analyses were performed to assess the associations among age, Expanded Disability Status Scale (EDSS), and the Age-Related MS Severity Score (ARMSS) with the volume of the different QSM lesion phenotypes. The following variables were used as confounding factors: for age, the total lesion volume, sex, and MS phenotypes; for EDSS, the total lesion volume, sex, age and MS phenotypes; for ARMSS, the total lesion volume, sex and MS phenotypes.

Data Availability

Data may be provided to interested researchers on request to the corresponding author, after clearance from the ethics committee.

RESULTS

Demographic and Clinical Features

Of the 53 patients with MS, 34 (64.2%) were women, and 40 (75.5%) had relapsing-remitting MS. Table 1 reports the main demographic and disease-related characteristics. Mean age and disease duration were 43.64 (SD, 12.58) years and 9.91 (SD, 10.56) years, respectively. The median EDSS was 2.0 (range, 0–7.0). The mean ARMSS was 3.99 (SD, 2.32). Nine patients (17%) were not receiving any disease-modifying therapy, 10 patients (19%) were treated with low-efficacy disease-modifying therapy, and the remaining 34 (64%) were on high-efficacy disease-modifying therapy. HCs were 24 (of which, 16 were women) with a mean age of 38.12 (SD, 13.2) years. No significant differences were found in age and sex between patients with MS and HCs.

MS Lesion Classification

No new MS lesions were observed compared with the most recent clinical MR imaging examination available before study entry. A total of 932 supratentorial WM lesions were examined using QSM and SMWI (Figs 1 and 2). Thirty-six lesions (3.8%) were excluded because of artifactual distortion (15 lesions), basal ganglia involvement (5 lesions), and confluent shape with a heterogeneous intensity pattern, which would not allow a proper classification (16 lesions). The remaining 896 lesions were first individually assessed and divided into 3 groups on the basis of the QSM signal: 320 ISO-HYPO, 475 HYPER, and 101 PRLs. SMWI was used to exclude lesions in which the presence of blood vessels in the lesion was a confounding element. A total of 52 lesions (5.8% of the total, all belonging to the HYPER group) were excluded due to the prominence of blood vessels within the lesion. Furthermore, after SMWI inspection, 55 lesions of the remaining HYPER group were assigned to the ISO-HYPO group because their inhomogeneous hyperintense signal was actually imputable to vessels. Similarly, 36 lesions (35.6% of the PRLs) shifted from PRLs to the HYPER group because the hyperintense rim was ascribable to the presence of vessels. Examples of the SMWI reclassification are shown in Fig 2. The final classification consisted of

- ISO-HYPO lesions, 375/844 (44.4%)
- HYPER lesions, 404/844 (47.9%)
- PRLs, 65/844 (7.7%).

In summary, the adoption of SMWI to support the allocation of lesions to appropriate categories resulted in a 35.6% decrease in the number of PRLs, a 22.5% decrease of HYPER, and a 17.2% increase in the number of ISO-HYPO, with respect to the categorization based on QSM only. In total, of the 896 lesions that were examined using QSM and SMWI, 135 lesions (15.1%) required a second evaluation to reach a consensus between the raters.

Quantitative analysis of the QSM signal confirmed that ISO-HYPO had significantly lower QSM values compared with HYPER and PRLs ($P < .001$ for both comparisons). HYPER and PRLs showed similar, though heterogeneous, QSM values ($P = .567$). ISO-HYPOs values were significantly smaller than those in HYPER and PRLs ($P < .001$ for both comparisons)

Table 2: Comparison of lesion volume and quantitative MR imaging values of the 3 lesion phenotypes

	ISO-HYPO (Mean) (SD)	HYPER (Mean) (SD)	PRL (Mean) (SD)	ISO-HYPO vs HYPER (P Value)	ISO-HYPO vs PRL (P Value)	HYPER vs PRL (P Value)
Lesion volume (μL)	311.44 (1069.32)	820.93 (1733.99)	955.35 (891.77)	<.001[a]	<.001[a]	.455
ICVF	0.47 (0.09)	0.42 (0.08)	0.41 (0.08)	<.001[a]	<.001[a]	.188
ODI	0.23 (0.07)	0.21 (0.06)	0.22 (0.05)	.060	.506	.703
FWF	0.03 (0.03)	0.04 (0.05)	0.07 (0.07)	.006[a]	<.001[a]	<.001[a]
MWF	0.075 (0.035)	0.068 (0.031)	0.062 (0.030)	.016[a]	.022[a]	.336
T1-relaxometry (ms)	1027.05 (131.35)	1077.18 (157.63)	1181.43 (157.01)	.001[a]	<.001[a]	<.001[a]
QSM values (ppb)	−9.10 (23.7)	9.06 (25.1)	7.75 (23.5)	<.001[a]	<.001[a]	.567
Distance from ventricular CSF (mm)	14.6 (9.8)	12.5 (9.7)	10.5 (7.4)	.059	.018[a]	.177

Note:—ppb indicates parts per billion.
[a] Statistically significant.
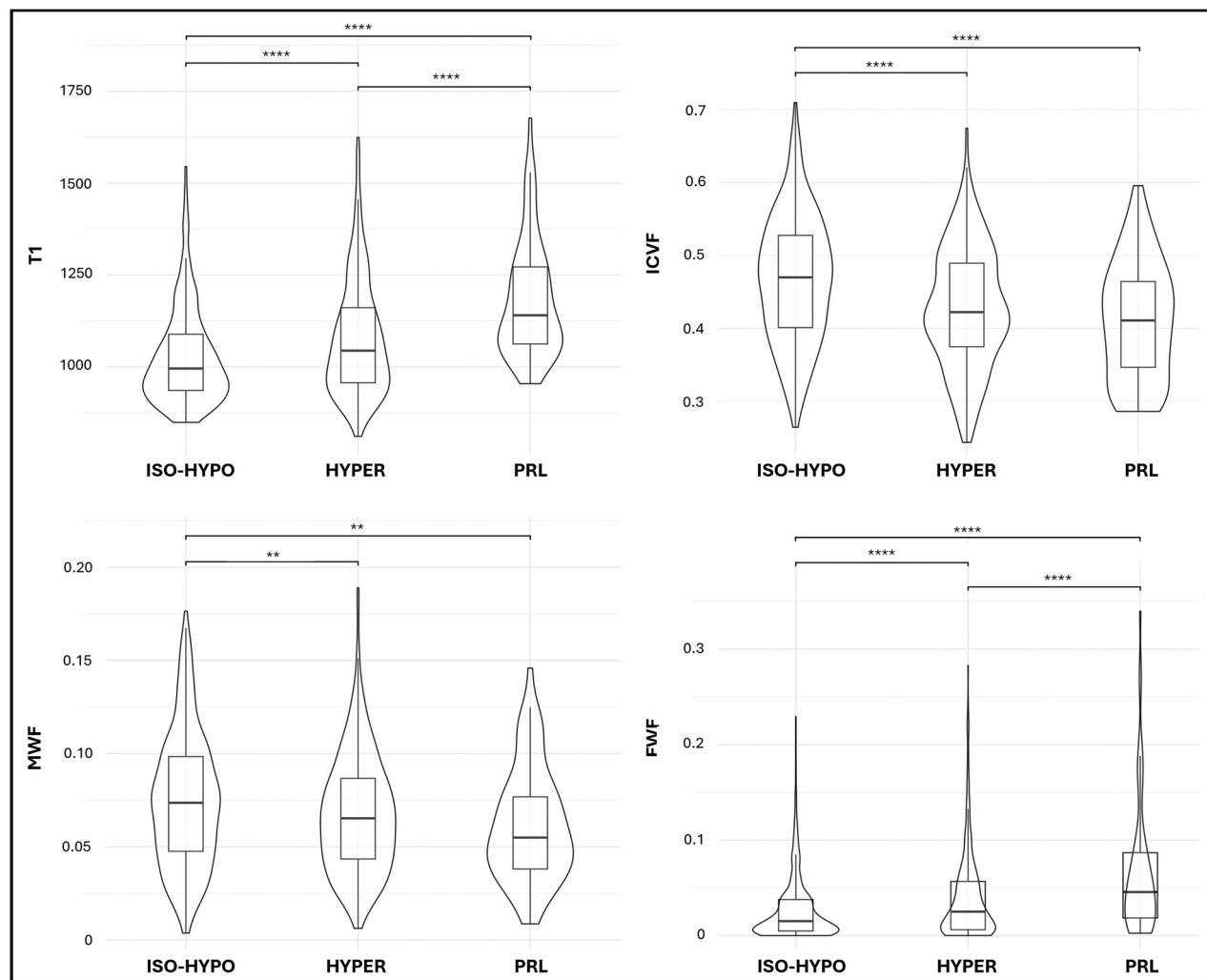
FIG 3. Quantitative MR imaging metrics of myelin and axonal loss in different MS lesion phenotypes. Comparisons were performed using ANOVA with Bonferroni post hoc comparisons, controlling for age, sex, lesion volume, and subject identification as confounding factors. T1-relaxation times are expressed in milliseconds. **$P \leq .05$; ****$P < .001$.

(Table 2). No differences in lesion volumes were observed between HYPER and PRLs.

Microstructural Characterization and Localization of Different MS Lesion Phenotypes

Figure 3 and Table 2 illustrate the results of the quantitative MR imaging analyses for the 3 lesion phenotypes. A worsening gradient ISO-HYPO→HYPER→PRLs in the T1-relaxation time was detected, with longer T1 times observed in PRLs compared with the other lesion groups ($P < .001$ in comparison with both ISO-HYPO and HYPER). The same continuum was observed for FWF values, with a significantly higher FWF in PRLs with respect to the other lesion groups ($P < .001$ for both comparisons). Accordingly, the MWF was reduced in PRLs and

Table 3: Pearson correlation among age, EDSS, and ARMSS with the volume of the different MS lesion phenotypes

	ISO-HYPO		HYPER		PRL		HYPER + PRL	
	r	P Value	r	P Value	r	P Value	r	P Value
Age	0.045	.763	−0.060	.689	−0.015	.920	−0.082	.583
EDSS	−0.180	.232	0.282	.057	−0.160	.289	0.228	.127
ARMSS	−0.268	.079	0.382	.011[a]	−0.167	.277	0.342	.023[a]

[a] Statistically significant.

HYPER compared with ISO-HYPO ($P < .016$ comparing HYPER with ISO-HYPO and $P < .022$ comparing PRLs with ISO-HYPO). The ICVF was significantly reduced in HYPER and PRLs compared with ISO-HYPO ($P < .001$ for both groups of comparisons). No differences were found in MWF and ICVF values comparing PRLs and HYPER (respectively $P = .336$ and $P = .188$). Furthermore, no differences were observed in ODI among the 3 lesion phenotypes.

Table 2 also reports the mean distance from the ventricular CSF of each lesion phenotype. ISO-HYPO were located farther away from the ventricles than PRLs ($P = .018$), which were the type of MS lesions closest to the ventricles.

Associations with Clinical Outcomes

As shown in Table 3, no correlations were observed among the volumes of ISO-HYPO, HYPER and PRLs, age and EDSS. No differences were noted among MS phenotypes or between men and women. A significant positive correlation was found between a worse ARMSS and higher HYPER volume ($P = .011$, $r = 0.382$) as well as between a worse ARMSS and the combined volume of HYPER and PRLs ($P = .023$, $r = 0.342$). Finally, a trend between a better ARMSS and higher ISO-HYPO volume was observed ($P = .079$, $r = −0.268$).

DISCUSSION

In this study, we classified MS lesions on the basis of QSM and SMWI and characterized them using T1-relaxometry, diffusion imaging, and myelin mapping. The 3 types of MS lesions (ISO-HYPO, HYPER, and PRL) were characterized by increasing degrees of axonal and myelin damage assessed with multimodal quantitative MR imaging. The use of SMWI enabled avoiding misclassification of MS lesions as HYPER and/or PRL because of the presence of veins, thus providing a more robust classification of MS lesions based on the QSM signal arising from the lesion itself. Our data confirm and extend the results from the pivotal study of Rahmanzadeh et al,[8] showing that PRLs have the lowest MWF and ICVF, supporting in vivo evidence that proinflammatory microglia contribute to ongoing demyelination and axonal loss. In this study, we combined T1-relaxometry and QSM, showing that PRLs also have longer T1-relaxation times, suggesting irreversible tissue damage, supporting recent findings.[12] We also observed that lesions with iso-/hypointense QSM, proposed as a biomarker of remyelinated lesions,[8] are characterized by significantly shorter T1-relaxation times than all other MS lesions. This finding is in line with data from Kolb et al,[13] who found that a shorter T1-relaxation time was strongly related to a higher remyelination degree at postmortem histology. To the best of our knowledge, this is the first study showing a direct relationship between T1-relaxometry

and QSM in identifying remyelinated lesions in the same cohort of patients. The mutual validation of these techniques is of great importance because it opens the possibility of adopting isointense lesions in T1 and QSM as a biomarker for remyelination in future studies investigating in vivo the remyelinating potential of novel drugs.

We confirm that a broad spectrum of hyperintensity patterns in MS lesions exists, encompassing a continuum that spans from a uniform pattern to diffuse inhomogeneous signal and scattered hyperintensities.[36] The underlying biologic rationale behind these diverse hyperintensity patterns remains uncertain. It is plausible that a substantial number of lesions classified as QSM-hyperintense might feature intricate vasculature, particularly in vein-rich regions like the periventricular areas. In this study, 55 lesions were initially classified as HYPER using QSM only and were finally classified as ISO-HYPO after examination of the corresponding SMWI, which allowed a better visualization of veins. Similarly, 36 lesions initially categorized as PRLs were ultimately reclassified as HYPER after inspection with SMWI. This finding is particularly intriguing because it suggests that 35.6% of the lesions initially classified as PRLs based on QSM visual inspection were later determined not to be PRLs after a meticulous evaluation of vessel presence. These findings might provide an explanation for the substantial variations observed in the frequencies of PRLs and other MS lesion phenotypes in prior studies, which used diverse MR imaging sequences and processing methods.

Our results underscore the necessity for a meticulous examination of veins when identifying PRLs and HYPER, particularly in the periventricular regions where numerous medullary veins are present. While there has been a recent attempt to establish a consensus for identifying PRLs,[10] the validation and standardization of MR imaging protocols for characterizing other MS lesion phenotypes remain incomplete. For example, the pathologic role of HYPER has not been completely described. In our study, HYPER showed a certain degree of microstructural damage and demyelination, and both ICVF and MWF could not distinguish them from PRLs unlike T1-relaxation time and FWF. Most interesting, we found that HYPER volume as well as the combined volume of HYPER+PRLs were associated with worse disease severity, as calculated with the ARMSS. Indeed, inhomogeneous, diffuse HYPER might mirror the presence of widespread inflammation or derive from the confluence of plaques with different degrees of inflammation or represent lesions with scattered foci of activated microglia not yet organized in a peripheral rim. This hypothesis is supported by the results of a recent PET/MR imaging study using [^{18}F]-DPA-714,[37] which revealed that more than one-half of MS lesions contain an inflammatory smoldering component (a frequency notably higher than solely attributed to PRLs). Similarly, Rahmanzadeh et al[8] found that 20% of all QSM-hyperintense lesions are chronically active at postmortem evaluation. Our quantitative MR imaging analyses support the idea that some HYPER might exhibit a diffuse inflammatory component, driving ongoing demyelination and tissue loss.

Several PET/MR imaging studies have indicated that lesions closer to the ventricles exhibit more inflammation and have a lower likelihood of remyelination compared with deep WM lesions.[2,6,38] Similarly, normal-appearing WM closer to the ventricles shows higher T1 values.[4] Here, we showed that PRLs were closer than ISO-HYPO to the ventricular CSF, supporting the hypothesis that the ventricular CSF might promote chronic inflammation within WM MS lesions, impairing efficient remyelination. Recently, a novel class of chronically active lesions, namely juxtacortical rim lesions, has been described.[39] Juxtacortical rim lesions have not been shown to have a clear relation with WM PRLs and might be closely linked to MS cortical pathology. Further studies are needed to elucidate if juxtacortical rim lesions are an expression of the detrimental activity of the peripheral subarachnoid CSF or if they are consequent to an alternative pathogenic mechanism.

One should consider the limitations of this study. Its cross-sectional design impedes the assessment of the evolution of the different lesion classes with time, and it is possible that the 3 lesion phenotypes are indeed representative of a dynamic continuum, with one phenotype evolving into another, which will be investigated in future studies. Moreover, the size of this patient cohort with mild clinical severity and diverse disease duration could have an influence on the observed correlations. Furthermore, the possible impact of different lesion phenotypes on the patient's degree of disability across time cannot be investigated without a longitudinal observation. For instance, in our study, the sum of HYPER and PRL volumes was associated with increased disability. This result was primarily driven by the number of lesions belonging to the HYPER class, but the limited number of PRLs may have influenced the lack of statistically significant correlation with clinical disability at the time of the MR imaging examination. The impact of PRLs might be better assessed with longitudinal observations. The absence of a direct pathologic correlation with imaging findings is another further limitation of this study.

CONCLUSIONS

Using a combined QSM and SMWI approach, we identified 3 classes of MS lesions, characterized by varying degrees of myelin and axonal loss. SMWI greatly improved lesion classification, allowing precise visualization of veins bordering or crossing the WM lesions. Using complementary quantitative MR imaging contrasts, we confirmed that PRLs are characterized by the most severe microstructural damage and myelin loss. On the contrary, ISO-HYPO show the highest MWF and shortest T1-relaxation time and ICVF, indicating lesions with less severe structural damage. Our in vivo results corroborate recent postmortem studies that demonstrated the association between ISO-HYPO and remyelination. Inflamed, demyelinated PRLs were more likely located close to the ventricles, while ISO-HYPO were more likely to occur in the deep WM, corroborating a surface-in theory in MS pathology and the possible presence of CSF toxic activity. The in vivo identification of the MS lesion heterogeneity could guide patients' stratification and prognosis.

REFERENCES

1. Kuhlmann T, Ludwin S, Prat A, et al. **An updated histological classification system for multiple sclerosis lesions.** *Acta Neuropathol* 2017;133:13–24 CrossRef Medline

2. Pardini M, Brown JWL, Magliozzi R, et al. **Surface-in pathology in multiple sclerosis: a new view on pathogenesis?** *Brain J Brain* 2021;144:1646–54 CrossRef Medline

3. Klistorner S, Barnett MH, Graham SL, et al. **The expansion and severity of chronic MS lesions follows a periventricular gradient.** *Mult Scler* 2022;28:1504–14 CrossRef Medline

4. Vaneckova M, Piredda GF, Andelova M, et al. **Periventricular gradient of T1 tissue alterations in multiple sclerosis.** *Neuroimage Clin* 2022;34:103009 CrossRef Medline

5. Marinero C, Louapre C, Govindarajan ST, et al. **Gradient in cortical pathology in multiple sclerosis by in vivo quantitative 7 T imaging.** *Brain* 2015;138(Pt 4):932–45 CrossRef Medline

6. Poirion E, Tonietto M, Lejeune FX, et al. **Structural and clinical correlates of a periventricular gradient of neuroinflammation in multiple sclerosis.** *Neurology* 2021;96:e1865–75 CrossRef Medline

7. Gillen KM, Mubarak M, Park C, et al. **QSM is an imaging biomarker for chronic glial activation in multiple sclerosis lesions.** *Ann Clin Transl Neurol* 2021;8:877–86 CrossRef Medline

8. Rahmanzadeh R, Galbusera R, Lu PJ, et al. **A new advanced MRI biomarker for remyelinated lesions in multiple sclerosis.** *Ann Neurol* 2022;92:486–502 CrossRef Medline

9. Ng Kee Kwong KC, Mollison D, Meijboom R, et al. **The prevalence of paramagnetic rim lesions in multiple sclerosis: a systematic review and meta-analysis.** *PLoS One* 2021;16:e0256845 CrossRef Medline

10. Bagnato F, Sati P, Hemond CC, et al. **Imaging chronic active lesions in multiple sclerosis: a consensus statement.** *Brain J Neurol* 2024 Jan 16 [Epub ahead of print] CrossRef Medline

11. Gho SM, Liu C, Li W, et al. **Susceptibility map-weighted imaging (SMWI) for neuroimaging.** *Magn Reson Med* 2014;72:337–46 CrossRef Medline

12. Krajnc N, Schmidbauer V, Leinkauf J, et al. **Paramagnetic rim lesions lead to pronounced diffuse periplaque white matter damage in multiple sclerosis.** *Mult Scler* 2023;29:1406–17 CrossRef Medline

13. Kolb H, Absinta M, Beck ES, et al. **7T MRI differentiates remyelinated from demyelinated multiple sclerosis lesions.** *Ann Neurol* 2021;90:612–26 CrossRef Medline

14. Hu H, Ye L, Ding S, et al. **The heterogeneity of tissue destruction between iron rim lesions and non-iron rim lesions in multiple sclerosis: a diffusion MRI study.** *Mult Scler Relat Disord* 2022;66:104070 CrossRef Medline

15. Piredda GF, Hilbert T, Thiran JP, et al. **Probing myelin content of the human brain with MRI: a review.** *Magn Reson Med* 2021; 85:627–52 CrossRef Medline

16. Mussard E, Hilbert T, Forman C, et al. **Accelerated MP2RAGE imaging using Cartesian phyllotaxis readout and compressed sensing reconstruction.** *Magn Reson Med* 2020;84:1881–94 CrossRef Medline

17. Piredda GF, Hilbert T, Canales-Rodríguez EJ, et al. **Fast and high-resolution myelin water imaging: Accelerating multi-echo GRASE with CAIPIRINHA.** *Magn Reson Med* 2021;85:209–22 CrossRef Medline

18. Sati P, Thomasson DM, Li N, et al. **Rapid, high-resolution, whole-brain, susceptibility-based MRI of multiple sclerosis.** *Mult Scler* 2014;20:1464–70 CrossRef Medline

19. Zhang F, Daducci A, He Y, et al. **Quantitative mapping of the brain's structural connectivity using diffusion MRI tractography: a review.** *Neuroimage* 2022;249:118870 CrossRef Medline

20. Caruyer E, Lenglet C, Sapiro G, et al. **Design of multishell sampling schemes with uniform coverage in diffusion MRI.** *Magn Reson Med* 2013;69:1534–40 CrossRef Medline

21. von Elm E, Altman DG, Egger M, et al. **The Strengthening the Reporting of Observational Studies in Epidemiology (STROBE) Statement: Guidelines for Reporting Observational Studies.** *Ann Intern Med* 2007;147:573–77 CrossRef Medline

22. Schofield MA, Zhu Y. **Fast phase unwrapping algorithm for inter-ferometric applications.** *Opt Lett* 2003;28:1194–96 CrossRef Medline

23. Schweser F, Deistung A, Lehr BW, et al. **Quantitative imaging of intrinsic magnetic tissue properties using MRI signal phase: an approach to in vivo brain iron metabolism?** *Neuroimage* 2011;54:2789–807 CrossRef Medline

24. Nam Y, Gho SM, Kim DH, et al. **Imaging of nigrosome 1 in substantia nigra at 3T using multiecho susceptibility map-weighted imaging (SMWI).** *J Magn Reson Imaging* 2017;46:528–36 CrossRef Medline

25. Bilgic B, Costagli M, Chan KS, et al; ISMRM Electro-Magnetic Tissue Properties Study Group. **Recommended implementation of quantitative susceptibility mapping for clinical research in the brain: a consensus of the ISMRM electro-magnetic tissue properties study group.** *Magn Reson Med* 2024;91:1834–62 CrossRef Medline

26. Jenkinson M, Beckmann CF, Behrens TEJ, et al. **FSL.** *Neuroimage* 2012;62:782–90 CrossRef Medline

27. Lim IA, Faria AV, Li X, et al. **Human brain atlas for automated region of interest selection in quantitative susceptibility mapping: application to determine iron content in deep gray matter structures.** *Neuroimage* 2013;82:449–69 CrossRef Medline

28. Lancione M, Tosetti M, Donatelli G, et al. **The impact of white matter fiber orientation in single-acquisition quantitative susceptibility mapping.** *NMR Biomed* 2017;30(11) CrossRef Medline

29. Canales-Rodríguez EJ, Pizzolato M, Piredda GF, et al. **Comparison of non-parametric T2 relaxometry methods for myelin water quantification.** *Med Image Anal* 2021;69:101959 CrossRef Medline

30. Veraart J, Novikov DS, Christiaens D, et al. **Denoising of diffusion MRI using random matrix theory.** *NeuroImage* 2016;142:394–406 CrossRef Medline

31. Andersson JLR, Sotiropoulos SN. **An integrated approach to correction for off-resonance effects and subject movement in diffusion MR imaging.** *Neuroimage* 2016;125:1063–78 CrossRef Medline

32. Avants BB, Tustison NJ, Song G, et al. **A reproducible evaluation of ANTs similarity metric performance in brain image registration.** *NeuroImage* 2011;54:2033–44 CrossRef Medline

33. Zhang H, Schneider T, Wheeler-Kingshott CA, et al. **NODDI: practical in vivo neurite orientation dispersion and density imaging of the human brain.** *Neuroimage* 2012;61:1000–16 CrossRef Medline

34. Daducci A, Canales-Rodríguez EJ, Zhang H, et al. **Accelerated Microstructure Imaging via Convex Optimization (AMICO) from diffusion MRI data.** *Neuroimage* 2015;105:32–44 CrossRef Medline

35. Marques JP, Kober T, Krueger G, et al. **MP2RAGE, a self bias-field corrected sequence for improved segmentation and T1-mapping at high field.** *NeuroImage* 2010;49:1271–81 CrossRef Medline

36. Hemond CC, Reich DS, Dundamadappa SK. **Paramagnetic rim lesions in multiple sclerosis: comparison of visualization at 1.5-T and 3-T MRI.** *AJR Am J Roentgenol* 2022;219:120–31 CrossRef Medline

37. Hamzaoui M, Garcia J, Boffa G, et al. **Positron emission tomography with [18F]-DPA-714 unveils a smoldering component in most multiple sclerosis lesions which drives disease progression.** *Ann Neurol* 2023;94:366–83 CrossRef Medline

38. Tonietto M, Poirion E, Lazzarotto A, et al. **Periventricular remyelination failure in multiple sclerosis: a substrate for neurodegeneration.** *Brain* 2023;146:182–94 CrossRef Medline

39. Galbusera R, Bahn E, Weigel M, et al. **Characteristics, prevalence, and clinical relevance of juxtacortical paramagnetic rims in patients with multiple sclerosis.** *Neurology* 2024;102:e207966 CrossRef Medline